

# The removal of a disulfide bridge in CotA-laccase changes the slower motion dynamics involved in copper binding but has no effect on the thermodynamic stability

André T. Fernandes · Manuela M. Pereira · Catarina S. Silva ·  
Peter F. Lindley · Isabel Bento · Eduardo Pinho Melo ·  
Lígia O. Martins

Received: 1 December 2010 / Accepted: 8 February 2011  
© SBIC 2011

**Abstract** The contribution of the disulfide bridge in CotA-laccase from *Bacillus subtilis* is assessed with respect to the enzyme's functional and structural properties. The removal of the disulfide bond by site-directed mutagenesis, creating the C322A mutant, does not affect the spectroscopic or catalytic properties and, surprisingly, neither the long-term nor the thermodynamic stability parameters of the enzyme. Furthermore, the crystal structure of the C322A mutant indicates that the overall structure is essentially the same as that of the wild type, with only slight alterations evident in the immediate proximity of the mutation. In the mutant enzyme, the loop containing the C322 residue becomes less ordered, suggesting perturbations to the substrate binding pocket. Despite the wild type and the C322A mutant showing similar thermodynamic stability in equilibrium, the holo or apo forms of the mutant unfold at faster rates than the wild-type enzyme. The

picosecond to nanosecond time range dynamics of the mutant enzyme was not affected as shown by acrylamide collisional fluorescence quenching analysis. Interestingly, copper uptake or copper release as measured by the stopped-flow technique also occurs more rapidly in the C322A mutant than in the wild-type enzyme. Overall the structural and kinetic data presented here suggest that the disulfide bridge in CotA-laccase contributes to the conformational dynamics of the protein on the microsecond to millisecond timescale, with implications for the rates of copper incorporation into and release from the catalytic centres.

**Keywords** Multicopper oxidases · Laccases · Protein stability and dynamics · Disulfide bridges · CotA-laccase

## Introduction

The family of multicopper oxidases (MCOs), which includes the functional classes of metallooxidases and laccases, is mostly constituted by proteins that contain approximately 500 amino acid residues and are composed of three Greek key  $\beta$ -barrel cupredoxin domains (domains 1, 2 and 3) that come together to form three spectroscopically distinct types of copper sites, i.e. type 1 (T1), type 2 (T2), and type 3 (T3) [1, 2]. The T1 copper centre is the site of substrate oxidation and a wide range of compounds, such as polyphenols, diamines and even some inorganic metals, are electron donor substrates. The trinuclear centre comprises two T3 copper ions and one T2 copper ion that functionally cooperate in the reduction of dioxygen to water. Laccases have a high potential for biotechnological applications, mainly owing to their wide range of oxidizing substrates, the use of readily available oxygen as the final electron acceptor and the lack of requirement for expensive

A. T. Fernandes · M. M. Pereira · C. S. Silva ·  
P. F. Lindley · I. Bento · L. O. Martins (✉)  
Instituto de Tecnologia Química e Biológica,  
Universidade Nova de Lisboa, Av. da República,  
2780-157 Oeiras, Portugal  
e-mail: lmartins@itqb.unl.pt

P. F. Lindley  
Department of Crystallography, Birkbeck College,  
University of London,  
Malet St., London WC1E 7HX, UK

E. P. Melo (✉)  
Centre for Molecular and Structural Biomedicine,  
Institute for Biotechnology and Bioengineering,  
Universidade do Algarve,  
Campus de Gambelas,  
8005-139 Faro, Portugal  
e-mail: emelo@ualg.pt

cofactors. In the past few years many studies have enabled the elucidation of a significant number of structural and functional aspects of these enzymes, but many questions still remain. One of these involves the understanding of the molecular determinants of enzyme long-term and conformational stability. However, using an enzyme in an industrial environment requires high stability, since most industrial activities are carried out at high temperatures, extreme pH values and high pressures, among other adverse physicochemical conditions. Therefore, understanding the molecular mechanisms involved in the stability properties of laccases is of utmost importance and may lead to the generation of improved biocatalysts by protein engineering techniques.

In recent years our attention has focused on the study of thermostable and hyperthermostable prokaryotic MCOs, the CotA-laccase from *Bacillus subtilis* and the metallo-oxidases McoA from *Aquifex aeolicus* and McoP from *Pyrobaculum aerophilum* [3–5]. These enzymes are all thermoactive ( $T_{\text{opt}} > 75$  °C) and remarkably thermostable, with melting temperatures between 80 and 114 °C [3, 5–7]. Copper was identified as a major determinant of the long-term and thermodynamic stability of CotA-laccase and McoA [6, 7], in agreement with previous studies performed with the eukaryotic MCOs ascorbate oxidase, human ceruloplasmin, yeast Fet3p and the laccases from *Rhus vernicifera* and *Coriulus hirsutus* [8–12]. Unfolding kinetics measured by the stopped-flow technique revealed that McoA aggregates under unfolding conditions, an uncommon feature among proteins, and this was further confirmed by light scattering, gel filtration and ANS binding [7]. The kinetic partitioning between aggregation and unfolding should be the main factor behind the low chemical stability of McoA at room temperature (2.8 kcal mol<sup>-1</sup>) and its low heat capacity change ( $\Delta C_p = 0.27$  kcal mol<sup>-1</sup> °C<sup>-1</sup>) [7]. This leads to a flat dependence of stability on temperature and explains the hyperthermostable nature of this enzyme. On the other hand, CotA-laccase, despite the narrower dependence of stability on temperature, shows remarkable chemical stability towards chemical denaturation (an energy gap of approximately 10 kcal mol<sup>-1</sup> at room temperature) [13] and therefore is more thermodynamically stable in the thermophilic temperature range (unpublished data). Furthermore, point mutations close to the T1 copper centre of CotA-laccase have a profound impact on the thermodynamic stability of the enzyme without causing major structural changes in the tertiary structure [6, 13].

In the present study the long-standing topic of the role of disulfide bonds in protein stability is revisited for CotA-laccase. Disulfide bridges, according to the classical theories, confer stability by reducing the conformational entropy of the unfolded state relative to the native state,

thereby decreasing the entropy gain upon unfolding [14–17]. The single intradomain disulfide bridge of the enzyme CotA-laccase from *B. subtilis* was disrupted, and the mutant C322A was characterized by using spectroscopic methods and fast kinetics of unfolding and of copper binding or release. Most of the studies on copper proteins using stopped-flow kinetics were confined to the simplest T1 copper proteins azurin and rusticyanin [18–20]. Overall, the data presented show that the disulfide bridge has no significant effect on the three-dimensional structure, catalytic properties and thermodynamic stability of CotA but contributes to its conformational dynamics on the microsecond to millisecond timescale, with implications for the rates of copper incorporation into and release from the catalytic centres. This study contributes to our understanding of the mechanisms of copper incorporation in MCOs.

## Materials and methods

### Construction of the C322A mutant

Single amino acid substitution in one of the cysteines (C322A) involved in the disulfide bridge of CotA-laccase was created using the QuikChange site-directed mutagenesis kit (Stratagene). Plasmid pLOM10 (containing the wild-type *cotA* sequence) was used as a template and the forward primer 5'-GCA AAC AGC GCG GGC AAC GGC GGT GAC GTC AAT C-3' and the reverse primer 5'-GAT TGA CGT CAC CGC CGT TGC CCG CGC TGT TTG C-3' were used to generate the C322A mutant. The presence of the desired mutation in the resulting plasmid and the absence of unwanted mutations in other regions of the insert were confirmed by DNA sequence analysis. The recombinant plasmid was transformed into *Escherichia coli* Tuner (DE3) strain (Novagen) to obtain strain AH3551.

### Overproduction and purification

Strains AH3551 (containing the gene *cotA* with the point mutation C322A) and AH3517 (containing the wild-type *cotA* gene [5]) were grown in Luria–Bertani medium supplemented with ampicillin (100 mg/mL) at 30 °C. Growth was monitored until the optical density at 600 nm was 0.6, at which time 0.1 mM isopropyl-β-D-thiogalactopyranoside and 0.25 mM CuCl<sub>2</sub> were added to the culture medium and the temperature was lowered to 25 °C. Incubation was continued for a further 4 h, when a change to microaerobic conditions was achieved [6]. Cells were harvested by centrifugation (8,000g, 10 min, 4 °C) after a further 20 h. For the overproduction of the apo-CotA forms, no copper

was added to the culture medium [6]. Proteins were purified by using a two-step purification procedure as previously described [5, 21].

#### UV-vis, EPR and circular dichroism spectra

Protein samples were routinely oxidized using potassium iridate followed by dialysis. UV-vis spectra were recorded using a Nicolet Evolution 300 spectrophotometer from Thermo Industries. The EPR spectra were measured with a Bruker EMX spectrometer equipped with an Oxford Instruments ESR-900 continuous-flow helium cryostat. The spectrum obtained under non-saturating conditions was theoretically simulated using the Aasa and Vännigard approach [22]. A circular dichroism spectrum in the far-UV region was measured with a JASCO (Tokyo, Japan) 720 spectropolarimeter using a circular quartz cuvette with a 0.01-cm optical path length in the range from 190 to 250 nm.

#### Enzymatic assays

The oxidation reactions of 2,2'-azinobis(3-ethylbenzo-6-thiazolinesulfonic acid) (ABTS) and syringaldazine were photometrically monitored with either a Nicolet Evolution 300 spectrophotometer from Thermo Industries or a Molecular Devices Spectra Max 340 microplate reader with a 96-well plate. All procedures were carried out as previously described [13].

#### Crystallization and structure solution

Crystals of the C322A mutant protein were obtained from a crystallization solution containing 12% PEG MME5k, 0.1 M sodium citrate at pH 5.5 and 16% 2-propanol, using the vapour diffusion method. Crystals were harvested after 6 days and cryoprotected in a solution containing the crystallization solution plus 22% ethylene glycol. Data collection, from a flash-cooled crystal, was undertaken on beam line ID13-EH1 at the European Synchrotron Radiation Facility in Grenoble, France, and a data set with 2.25 Å resolution was obtained. Diffraction data were processed and scaled using MOSFLM [23, 24] and SCALA, from the CCP4 suite [25], respectively (data collection statistics are listed in Table 1). The three-dimensional structure of the mutant protein was solved by the molecular replacement method using the program MOLREP [26] and as a search model, the structure of the native CotA (1W6L) [21], from which the solvent molecules as well as the copper ions had been removed. Refinement of the structural model was undertaken with the program REFMAC [27] and model building and improvement were performed with the program COOT [28]. Isotropic refinement of the atomic

**Table 1** Data collection and refinement statistics for the C322A mutant protein

Data collection statistics	
Beam line at ESRF	ID23-EH1
Wavelength (Å)	0.9537
Detector distance (mm)	331.6
Resolution (Å)	2.25
Space group	<i>P</i> 3 <sub>1</sub> 21
Cell parameters (Å)	
<i>a</i>	101.6
<i>c</i>	136.8
Mosaicity (°)	0.4
Oscillation angle (°)	0.65
Oscillation range (°)	63.05
No. of unique <i>hkl</i> reflections	36,605 (5,265)
Completeness (%)	99.9 (100.0)
<i>I</i> / <i>σ</i> ( <i>I</i> )	7.0 (2.1)
<i>R</i> <sub>sym</sub>	0.075 (0.349)
Multiplicity	3.7 (3.8)
Refinement statistics	
No. of protein atoms	4,120
No. of solvent atoms	402
No. of heteroatoms	4Cu + 2O + 6EDO
Final <i>R</i> factor	0.162
Final free <i>R</i> factor	0.206
Mean <i>B</i> values (Å <sup>2</sup> )	
Protein	35.4
Solvent	41.6
Overall	36.0
Estimated overall coordinate uncertainty (Å) <sup>a</sup>	0.104
Distance deviations <sup>b</sup>	
Bond distances (Å)	0.010
Bond angles (Å)	1.232
Planar groups (Å)	0.005
Chiral volume deviation (Å <sup>3</sup> )	0.079
Quality of models	
Ramachandran analysis (%)	
Favourable	96.4
Generous	3.6
Disallowed	0.0

Values in parentheses refer to the highest-resolution shells as follows: C322A (2.37–2.25 Å). Ramachandran analysis was determined by PROCHECK [55]

ESRF European Synchrotron Radiation Facility, EDO ethylene glycol

<sup>a</sup> Based on maximum likelihood

<sup>b</sup> Rms deviations from standard values

displacement parameters was performed for all atoms. The occupancies of the copper ions were adjusted so that their isotropic thermal vibration parameters refined approximately to those observed for the neighbouring atoms.

Solvent molecules were positioned after a few cycles of refinement as were several molecules of ethylene glycol. To model the species observed between the T3 copper sites, careful analysis of the omit and standard difference Fourier syntheses as well as of thermal vibration coefficients was undertaken, and a diatomic species was identified at this site [29]. The model giving the best refinement corresponded to a dioxygen moiety with the O–O distances constrained to the target value of 1.204 Å. Such a moiety could be an  $O_2^{2-}$  species, a partially protonated version or a mixture of such states. Refinement statistics are listed in Table 1.

## Stability

Long-term thermostability was determined at 80 °C for an enzyme solution in 20 mM tris(hydroxymethyl)aminomethane (Tris)–HCl buffer, pH 7.6. At appropriated times, samples were withdrawn, cooled and immediately examined for residual activity following oxidation by ABTS as previously described [5]. The thermodynamic stability assessed by steady-state fluorescence was measured with a Cary Eclipse spectrofluorimeter using 296 nm as the excitation wavelength. All proteins were in 20 mM Tris–HCl buffer at pH 7.6 and increasing concentrations of guanidine thiocyanate (GuSCN) were used to induce unfolding at 25 °C. Unfolding was measured by a combination of fluorescence intensity and the emission maximum and was quantified using two-state equations [13]. The stability of the tertiary structure was assessed by differential scanning calorimetry as previously described [6].

## Stopped-flow kinetics

Kinetic experiments were carried out with an Applied Photophysics Pi-Star 180 instrument with absorption and fluorescence intensity detection. A mixing ratio of 1:1 to give final protein concentrations of 2 and 20 μM for fluorescence and absorption detection, respectively, was used. The unfolding or refolding of proteins was followed by fluorescence with an excitation wavelength of 296 nm, and emission was detected above 320 nm using a glass filter. For the unfolding experiments the proteins in 20 mM Tris–HCl, pH 7.6, were mixed with 100 mM Britton-Robinson buffer, pH 1.6, to a final pH of 1.8. Copper release and binding was measured by absorption at 600 and 330 nm to probe the T1 and T3 copper ions, respectively. For copper binding experiments, the apo forms of proteins in 20 mM Tris–HCl, pH 7.6, were mixed with solutions ranging from 20 to 240 μM CuCl<sub>2</sub> in the same buffer. All kinetic traces were analysed according to a multiexponential fit using Pro-Data Viewer provided by Applied Photophysics.

## Other methods

The copper content of proteins was determined by the trichloroacetic acid/bicinchoninic acid method [30]. The protein concentration was measured using the CotA absorption band at 280 nm ( $\epsilon_{280} = 84,739 \text{ M}^{-1} \text{ cm}^{-1}$ ). Redox titrations were performed at 25 °C and pH 7.6, under an argon atmosphere, and were monitored by visible absorbance (300–900 nm) as described previously [13].

## Results and discussion

### Spectroscopic analysis

The recombinant C322A mutant shows the same chromatographic pattern during purification as wild-type CotA-laccase. Protein samples were judged to be homogeneous by the observation of a single band on sodium dodecyl sulfate polyacrylamide gel stained with Coomassie Blue. Each holoprotein “as isolated” contained approximately 4 mol copper per mole of protein. The UV–vis spectra of the wild type and the C322A mutant are very similar, having an intense absorption band at 600 nm ( $\epsilon = 4,000 \text{ M}^{-1} \text{ cm}^{-1}$ ) due to the charge transfer transition characteristic of the T1 copper centre (Fig. 1a). The EPR spectrum of the C322A mutant resembles that of the wild-type protein (i.e. the spin Hamiltonian parameters for the wild-type and mutant proteins for both T1 and T2 copper are similar; Fig. 1b). The circular dichroism spectrum of the mutant in the far-UV region reveals minimal changes in the secondary structure as compared with that of the wild type—the signal is dominated by  $\beta$ -sheets, turns and random coils and a small percentage of  $\alpha$ -helix (Fig. 1c). Overall, it seems that the C322A mutation results only in very subtle differences in the electronic structure of the copper centres.

### Redox and catalytic properties

The reduction of the T1 copper centre was monitored by the decrease of the  $S(\pi) \rightarrow \text{Cu}(d_{x^2-y^2})$  charge transfer absorption band at around 600 nm. The replacement of C322 by an alanine resulted in a decrease of the redox potential of the T1 copper centre ( $E_{\text{T}1}^{\text{o}}$ ) by approximately 70 mV (Table 2). The lower  $E_{\text{T}1}^{\text{o}}$  can reflect the variation of several factors, including the solvent accessibility and the electrostatic interactions between the metal centre and the protein [31]. The enzymatic kinetic constants ( $k_{\text{cat}}$  and  $K_m$ ) measured for the C322A mutant are similar to those exhibited by the wild-type enzyme (Table 2). The lower  $E_{\text{T}1}^{\text{o}}$  determined for the mutant enzyme would appear to

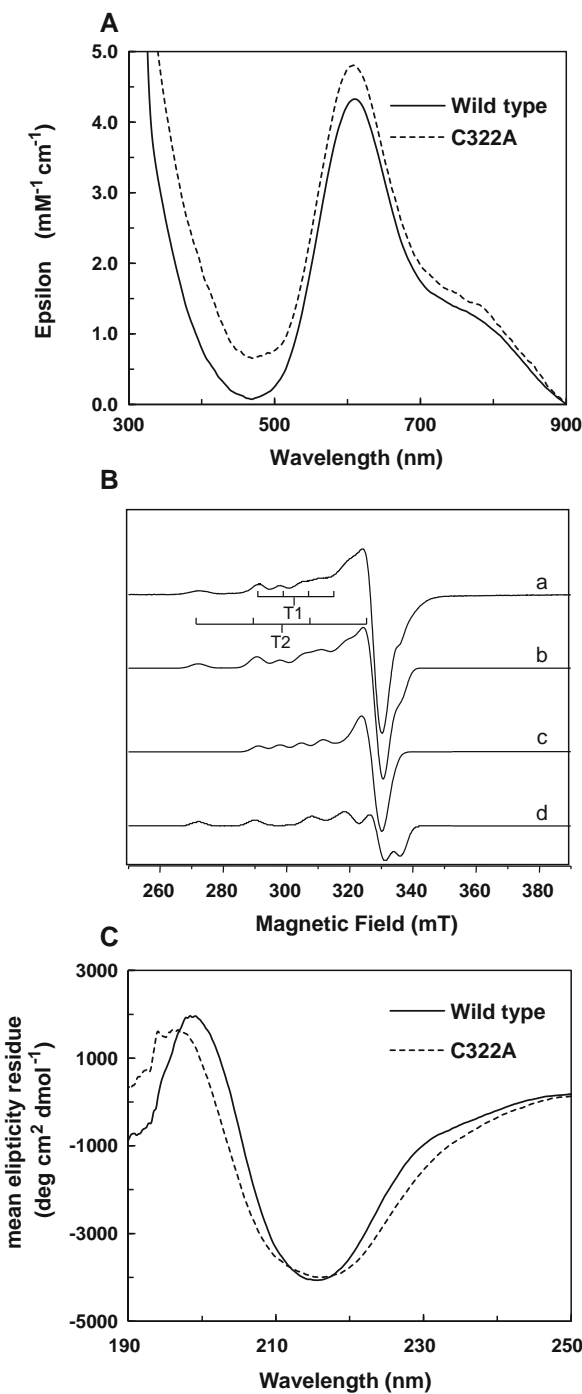


**Fig. 1** **a** UV-vis spectra of wild-type CotA and the C322A mutant in 20 mM Tris-HCl with 200 mM NaCl, pH 7.6. **b** EPR spectrum of the C322A mutant: the spectrum obtained at  $-263^{\circ}\text{C}$  with a microwave frequency of 9.39 GHz, microwave power of 2.4 mW and modulation amplitude of 0.9 mT (*a*); simulation of the total spectrum (*b*); and deconvolution of the different components (*c* and *d*). The parameters used were as follows: for type 1 (T1) copper  $g_{\min} = 2.042$ ,  $g_{\text{med}} = 2.046$ ,  $g_{\max} = 2.228$  and  $A_{\max} = 70 \times 10^{-4} \text{ cm}^{-1}$  and for type 2 copper (T2)  $g_{\min} = 2.035$ ,  $g_{\text{med}} = 2.094$ ,  $g_{\max} = 2.250$  and  $A_{\max} = 187 \times 10^{-4} \text{ cm}^{-1}$ . The contribution of the T1 and T2 components is 1:1 in the simulation of the total spectrum. The hyperfine splittings  $A_{\max}$  of the T1 and T2 copper centres are indicated. **c** Circular dichroism spectra in the far-UV region

**Table 2** Activation energy ( $\Delta G^{\pm}$ ), redox potential of the type 1 copper and steady-state kinetic constants for 2,2'-azinobis(3-ethylbenzo-6-thiazolinesulfonic acid) (ABTS) and syringaldazine (SGZ) for the wild type and the C322A mutant

	$\Delta G^{\pm}$ (kcal mol <sup>-1</sup> )	$E^{\circ}$ (mV)	ABTS		SGZ	
			$K_m$ ( $\mu\text{M}$ )	$k_{\text{cat}}$ ( $\text{s}^{-1}$ )	$K_m$ ( $\mu\text{M}$ )	$k_{\text{cat}}$ ( $\text{s}^{-1}$ )
Wild type	$2.9 \pm 0.1$	$525 \pm 10$	$102 \pm 1$	$264 \pm 9$	$8 \pm 2$	$79 \pm 4$
C322A	$4.2 \pm 0.9$	$457 \pm 5$	$105 \pm 9$	$238 \pm 17$	$8 \pm 0.3$	$73 \pm 1$

The activation energy was determined using ABTS as a substrate

favour a decreased reaction velocity as the rate of an electron transfer reaction ( $k_{\text{ET}}$ ) is a major component of  $k_{\text{cat}}$ , and is directly dependent on  $E^{\circ}$  [32]. However, according to the Marcus theory, two other factors affect the rate of an electron transfer reaction ( $k_{\text{ET}}$ ): the electronic tunnelling, which depends on the exact geometry of the protein matrix, and the reorganization energy, which depends on the structure and dynamics of the protein [31, 32]. Therefore, possible reasons for discrepancies in the reaction rate in relation to the redox potential of the C322A mutant must lie in the interplay among different and complex factors that are present in the catalytic mechanism of MCOs.

#### Thermodynamic stability characterization

The stability of CotA upon chemical-induced unfolding was evaluated by tryptophan fluorescence. The equilibrium curves at increasing concentrations of GuSCN show that the native state is more stable than the unfolded state by 5.5 and 5.4 kcal mol<sup>-1</sup> for the wild type and the C322A mutant, respectively, showing that the overall stability is maintained in the mutant despite the disruption of the disulfide bridge. Moreover, the other parameters that characterize the structural stability, namely the concentration of GuSCN at which 50% of the molecules are unfolded (midpoint) and the cooperativity of unfolding ( $m$ ), are similar for the wild-type and mutant proteins (Fig. 2a; Table 3).

The C322A mutant denatures irreversibly, according to a first-order process (Fig. 2b), pointing to a simple pathway of unfolding and deactivation, as described previously for the wild-type enzyme [5, 6]. At  $80^{\circ}\text{C}$  the C322A mutant has a slightly higher long-term stability than the wild type, with a half-life of inactivation of  $207 \pm 17$  min as compared with  $172 \pm 19$  min, but the error intervals overlap. The thermal stability was further probed by differential scanning calorimetry (Fig. 2c). The transitions obtained for the C322A mutant are as complex as those previously

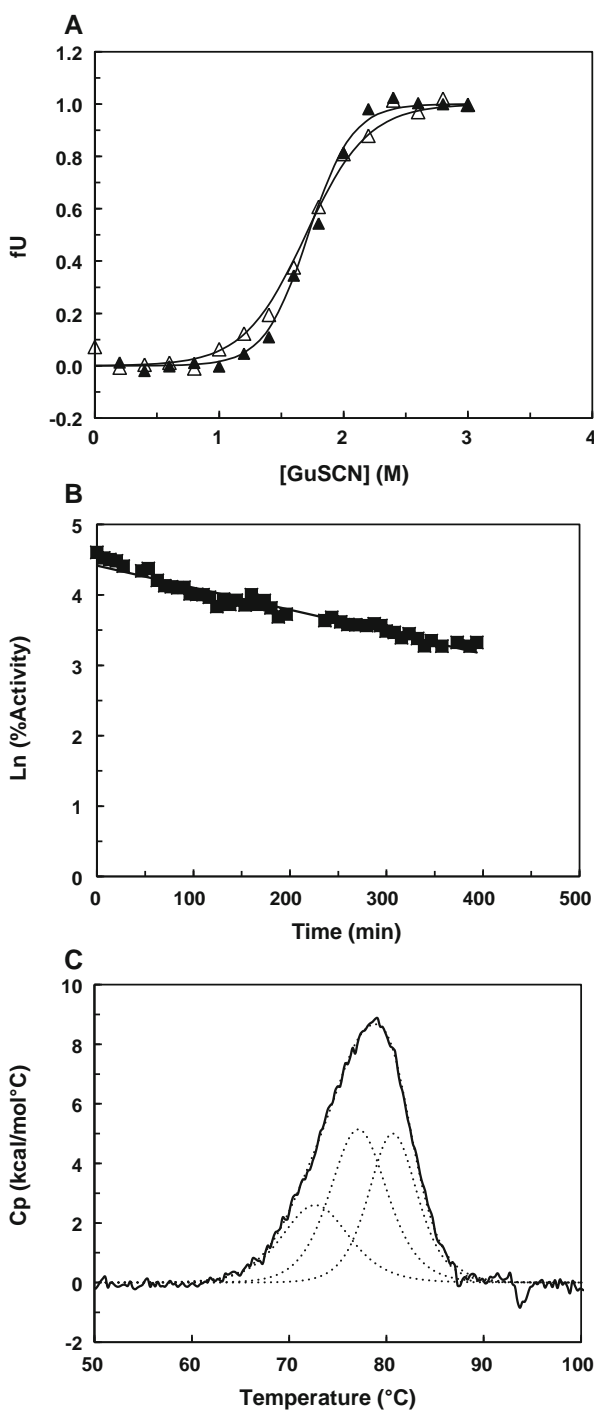


**Fig. 2** **a** Fraction of wild-type CotA (filled symbols) and C322A mutant (open symbols) unfolded ( $f_U$ ) by guanidine thiocyanate ( $GuSCN$ ) as measured by tryptophan fluorescence. The solid lines are the fits using the equation  $f_U = \exp(-\Delta G^0/RT)/1 + \exp(-\Delta G^0/RT)$ , which assumes the native  $\leftrightarrow$  unfolded equilibrium. **b** Long-term stability of the C322A mutant protein at 80 °C. **c** Differential scanning thermogram of the C322A mutant protein (solid line) fitted by three thermal transitions (dotted lines)

reported for the wild type and other MCOs, because aggregation occurs after the first scan, leading to 100% irreversibility of the process [3, 6, 7]. Moreover, the excess

**Table 3** Thermodynamic stability of the tertiary structure of wild-type CotA and the C322A mutant

	Wild type	C322A
$\Delta G^\circ$ (kcal mol <sup>-1</sup> )	$5.5 \pm 0.8$	$5.4 \pm 1.3$
$m$ (kcal mol <sup>-1</sup> )	$-3.4 \pm 0.6$	$-3.4 \pm 0.8$
Midpoint (M)	$1.6 \pm 0.1$	$1.6 \pm 0.1$

heat capacity could only be fitted using three calorimetric transitions, supporting sequential domain unfolding. The overall thermal stability of the C322A mutant is comparable to that of the wild type, with midpoint temperatures ( $T_m$ ) at each transition of 73, 78 and 81 °C. Overall, these results show that the disulfide bridge does not have a major contribution to the thermodynamic or the thermal stability of CotA-laccase.

#### Structural characterization

The three-dimensional structure of the C322A mutant was solved and the overall fold is very similar to that of the wild type (the rms deviation of the  $C\alpha$  trace is 0.618 Å). Similarly to the wild-type holo structure, the copper centres in the C332A mutant show full occupancies and a diatomic oxygen species was modelled in the trinuclear centre (Fig. 3a). Interestingly, in the mutant enzyme the loop that comprises residues 90–97, which is usually very poorly defined in previous CotA structures [21, 33], became less disordered and it was possible to model into the electron density maps residues 90–92 and 95–97. In the structure of the C322A mutant, the Cys229 residue becomes exposed to the solvent and appears to be chemically modified, and a methyl thiocysteine moiety was modelled at this position. A similar modification of exposed cysteine residues into oxycysteines has been observed in other CotA structures where the protein was produced following the microaerobic expression protocol [6]. In the wild type, the loop where Cys322 is involved in the disulfide bridge with Cys229 is well ordered and defined. In contrast, the most significant difference in the mutant structure is observed at the position of this loop, which becomes less ordered and moves some 8 Å away towards the solvent side (Fig. 3b). As the disulfide bridge is located at one of the edges of the substrate binding pocket, the mutation induces a slight change in the configuration of the binding pocket, and changes the substrate binding surface. This, in turn, may influence the incorporation of copper into the mononuclear T1 copper centre. This observation could contribute to the decreased  $E_{T1}^0$  determined for the C322A mutant [34]. Indeed, substitutions of hydrophobic residues with an alanine residue near the T1 copper of CotA-laccase in a previous study have been shown to increase the solvent

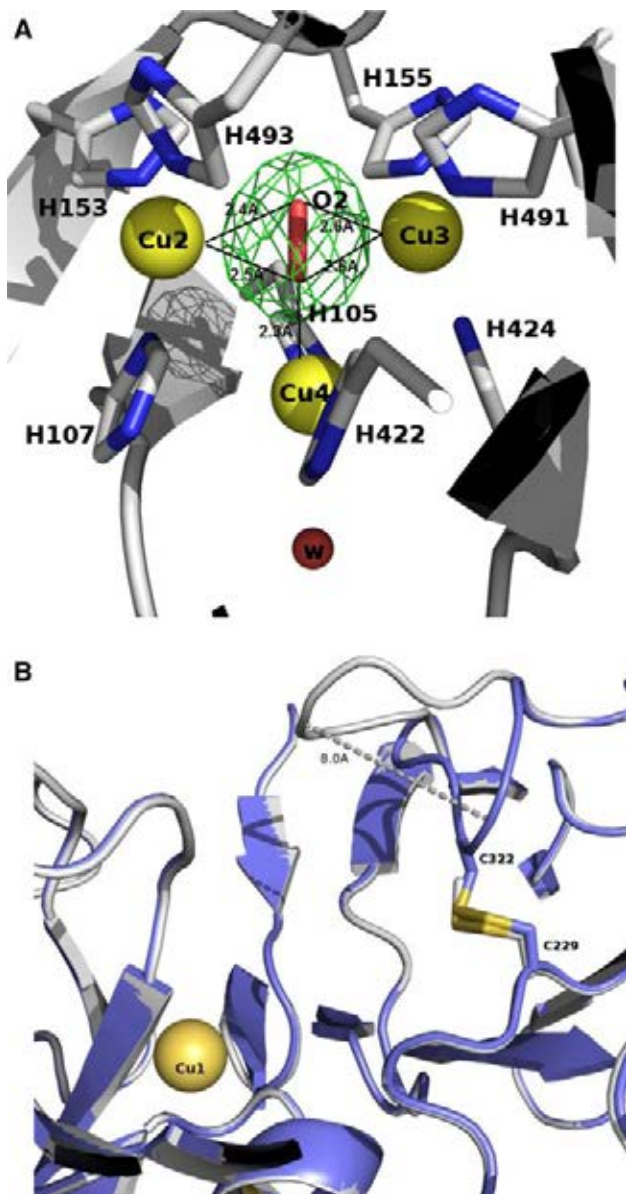


**Fig. 3** **a** Close-up view of the trinuclear centre in the C322A mutant structure. A difference Fourier synthesis contoured at the  $4\sigma$  level. **b** Superposition of the C $\alpha$  tracing of the C322A mutant protein and holo-Cota. The loop that contains residue 322 is coloured blue for the wild type and grey for the mutant. Residue 229 in the C322A mutant protein is coloured by atom type

accessibility and cause a decrease of the redox potential of the metal centre of the mutants [35].

#### Collisional quenching by acrylamide

To address possible modifications in the mutant protein dynamics, the accessibility of the tryptophan fluorophores was studied by using acrylamide as a fluorescence quencher (Fig. 4). The Stern–Volmer plots for the wild type and the C322A mutant are very similar, showing that

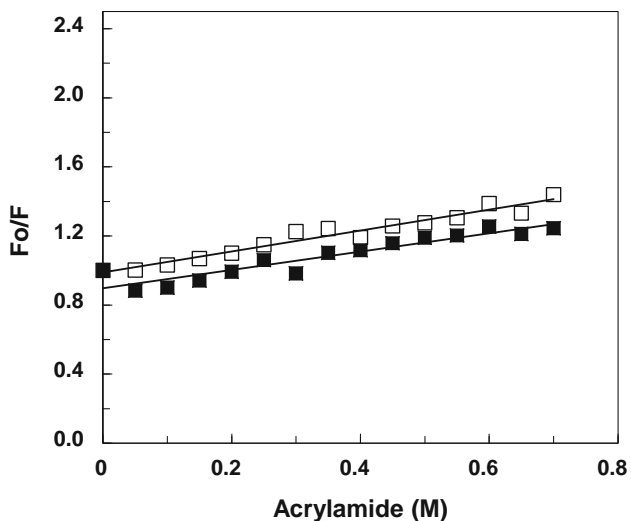


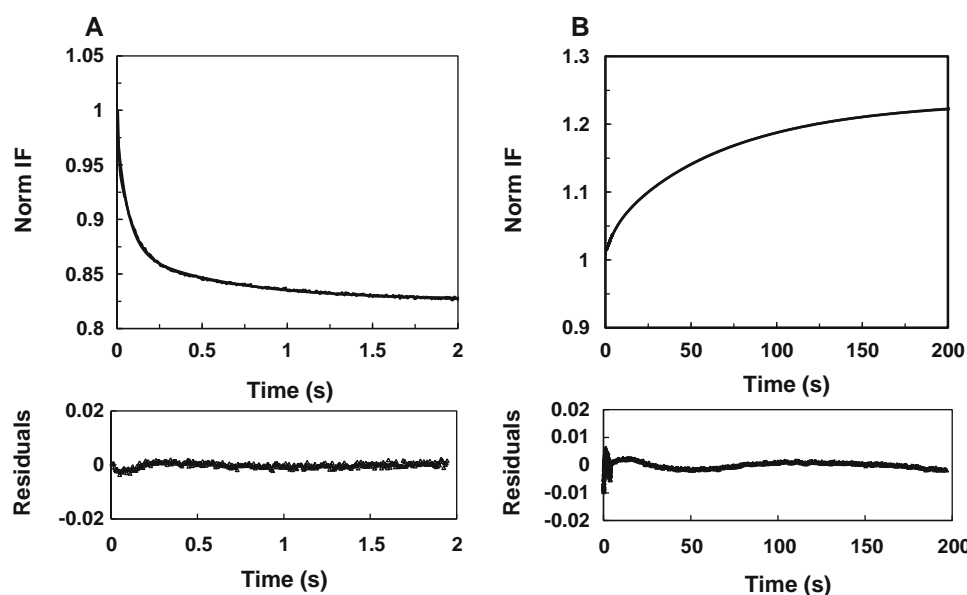
**Fig. 4** Stern–Volmer plot. Collisional quenching of wild-type CotA (filled squares) and of the C322A mutant (open squares)

the accessibility of tryptophan residues to acrylamide is similar in both proteins. The quenching of a fluorophore depends upon its “exposure” to the quencher. Indeed, a buried residue may occasionally expose itself to collisions with the quencher as a result of local or large-scale conformational fluctuations in the protein. Quenching of tryptophan fluorescence has to occur during the lifetime of the excited state and therefore only protein dynamics within this picosecond to nanosecond time range may allow tryptophan residues to collide with acrylamide. Therefore, collisional quenching also probes motion dynamics within the picosecond to nanosecond timescale of fluorescence lifetimes [36, 37] at least for tryptophan residues that are partially exposed at the protein surface [38]. The results obtained show that the disruption of the disulfide bridge in CotA-laccase does not affect protein dynamics on the picosecond to nanosecond timescale, which is generally defined as a fast timescale of protein motions.

#### Kinetics of the acid-induced unfolding

Unfolding kinetics as assessed by tryptophan fluorescence using the stopped-flow technique were measured using the apo and holo forms of the enzymes under study. Acidification was used to promote protein unfolding and, interestingly, it was observed that unfolding of the apo forms is characterized by a decrease in fluorescence, whereas unfolding of the holo forms was characterized by an increase in fluorescence (Fig. 5). This inversion of the fluorescence signal is most probably due to the assigned role of copper as a quencher of fluorescence [39]. The conformational unfolding of apo forms was fitted with a second-order exponential, whereas the unfolding of the

**Fig. 5** Unfolding induced by acid and assessed by tryptophan fluorescence. **a** Total fluorescence intensity variation of wild-type apo-CotA. **b** Total fluorescence intensity variation of wild-type holo-CotA. Kinetic traces were fitted with a double exponential for the apo form and with a triple exponential for the holo form as shown in the residuals plots



holo forms could only be accurately fitted by using a triple exponential (Table 4). This is most probably related to a higher complexity of the unfolding pathway in the holo forms, which certainly reflects the presence of copper ions at the catalytic centres. A lower number of unfolding phases, in apo forms, is also observed in other metalloproteins [40]. In the blue copper azurin, an unfolding pathway of higher complexity caused by a redox-active copper ion that remains bound to the protein in the unfolded state was observed [41]. The unfolding rates of the apo forms are almost 100-fold higher than those of the holo forms (Table 4), highlighting the effect of copper in stabilizing the protein three-dimensional structure. This stabilizing effect of copper could not be quantified through most classic approaches, such as equilibrium unfolding studies using chemical denaturants, because the enzymes become copper-depleted at low concentrations of denaturant prior to the overall unfolding [7, 13]. In consequence, the stabilizing effect of copper ion was calculated by applying the Arrhenius law (which accounts for the unfolding rates of the apo and holo forms) to each unfolding phase, for the mutant and the wild-type enzyme (Table 4) [42]. For these enzymes no major differences

were observed as the stabilizing effect for phase 1 ( $k_1$ ) is 1.6 and 1.8 kcal mol<sup>-1</sup> and for phase 2 ( $k_2$ ) is 0.2 and 0.3 kcal mol<sup>-1</sup> for wild-type CotA and the C322A mutant, respectively. These values are in the lower limit for the stabilizing effect of copper in the native state, i.e. assuming the absence of copper affinity in the transition state during unfolding, and are also in agreement with the spectroscopic and structural analysis, which revealed no major differences in the properties of the copper centres. Overall, the present results show that the C322A mutant globally unfolds faster than the wild-type enzyme. This suggests that the mutant most likely also refolds faster than the wild type, given that at the equilibrium the stability is not affected by the mutation (see above). However, owing to the occurrence of protein aggregation, the folding kinetics of these proteins could not be investigated.

#### Kinetics of copper release and binding

The rates of copper release from the T1 copper site were monitored upon acid-induced unfolding of the wild-type and C322A mutant holo forms. The kinetic traces measured at 600 nm were accurately fitted according to a double exponential (not shown), pointing to a complex process which might be a consequence of the centre reorganization, preceding the copper release from the T1 copper site (Table 5). The twofold higher decay rates at 600 nm in the C322A mutant as compared with the wild type indicate faster removal of the T1 copper ion in the mutant enzyme. The kinetic traces describing copper binding to the T1 and T3 sites of the apo forms, measured at 600 and 330 nm, respectively, required a triple exponential to be accurately fitted, despite the attempt to use pseudo-first-order

**Table 4** Values for the  $k_1$ ,  $k_2$  and  $k_3$  constants obtained from the fitting of kinetic traces reporting the variation in fluorescence intensity upon acid-induced unfolding

	$k_1$ (s <sup>-1</sup> )	$k_2$ (s <sup>-1</sup> )	$k_3$ (s <sup>-1</sup> )
Apo-CotA	$16.95 \pm 1.09$	$1.81 \pm 0.09$	—
Apo-C322A	$22.1 \pm 0.07$	$1.59 \pm 0.05$	—
Holo-CotA	$0.12 \pm 0.01$	$0.02 \pm 0.00$	$0.002 \pm 0.001$
Holo-C322A	$0.38 \pm 0.01$	$0.10 \pm 0.01$	$0.03 \pm 0.01$

**Table 5** Values for the  $k_1$  and  $k_2$  constants obtained from the fitting of kinetic traces reporting the decay of absorbance at 600 nm upon acid-induced unfolding

	$k_1$ ( $\text{s}^{-1}$ )	$k_2$ ( $\text{s}^{-1}$ )
Holo-CotA	$3.37 \pm 0.71$	$0.38 \pm 0.08$
Holo-C322A	$7.43 \pm 0.97$	$2.71 \pm 0.90$

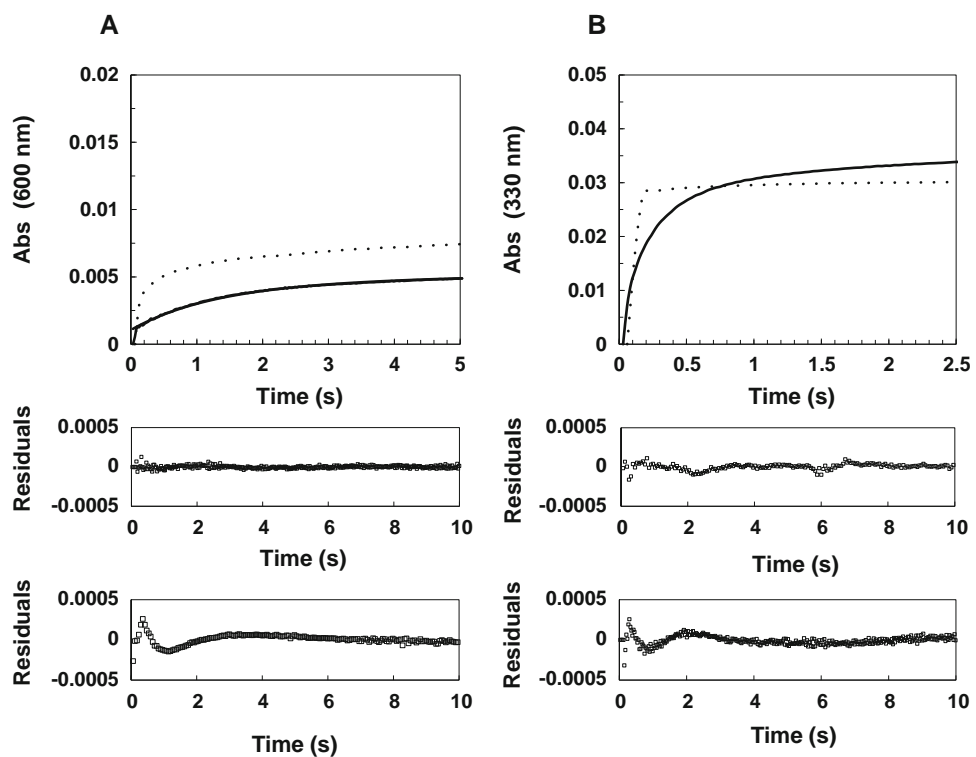
conditions (i.e. copper and apoprotein in a 10:1 ratio; Fig. 6; Table 6). These multiple rate constants might result from the presence of non-pseudo-first-order conditions or from binding followed by protein reorganization. Indeed, it has been recognized that metal binding to proteins may involve complex pathways with at least one intermediate during the binding process [43–46]. For example, in human ceruloplasmin it has been proposed that copper binding in vitro is a cooperative process presumably mediated by conformational changes transmitted within the protein upon copper binding [47]. On the other hand, copper binding to Sco from *B. subtilis*, a protein involved in the assembly of the Cu<sub>A</sub> centre in cytochrome *c* oxidase, is described by a two-step binding mechanism where the first step is a bimolecular process producing an intermediate that undergoes an isomerization step to yield the final holo form [44]. The fast rate constant  $k_1$  measured in the wild-type and mutant enzymes was assigned to the first bimolecular step of copper binding (Table 6). This rate was shown to be dependent on the copper concentration (data not shown). The C322A mutant has slightly faster rates of

copper binding followed at both 600 and 330 nm (Table 6). Interestingly, the rates of copper binding to the T1 centre are faster than the rates measured for copper binding to the T3 centre. This is in accordance with our previous results that pointed to a sequential process of copper incorporation into CotA-laccase, with the T1 copper centre being the first to be reconstituted, followed by the T2 and T3 copper centres [6], similarly to what occurs in CueO from *E. coli*, yeast Fet3P and human ceruloplasmin [48–50]. The differences observed in the rates of copper incorporation and release in the mutant enzymes as compared with the wild type should reflect subtle alterations in the protein dynamics, with consequences in structural unfolding rates and in the rates of copper release and incorporation. Only this slower motion regime and not the picosecond to nanosecond time range dynamics was affected as shown by acrylamide collisional fluorescence quenching analysis. The faster dynamics observed does not seem to affect copper coordination in the catalytic centres. In fact, and as

**Table 6** Values for the  $k_1$ ,  $k_2$  and  $k_3$  constants obtained from the fitting of kinetic traces reporting copper binding to the T1 and T3 sites (absorbance at 600 nm and 330 nm, respectively)

	$\lambda$ (nm)	$k_1$ ( $\text{s}^{-1}$ )	$k_2$ ( $\text{s}^{-1}$ )	$k_3$ ( $\text{s}^{-1}$ )
Apo-CotA	600	$20.1 \pm 6.05$	$0.78 \pm 0.02$	$0.09 \pm 0.004$
	330	$4.93 \pm 0.11$	$0.75 \pm 0.04$	$0.06 \pm 0.001$
Apo-C322A	600	$26.6 \pm 6.2$	$1.7 \pm 0.8$	$0.12 \pm 0.02$
	330	$10.4 \pm 0.15$	$1.4 \pm 0.02$	$0.08 \pm 0.008$

**Fig. 6** Copper binding to apo forms of the wild type (solid line) and the C322A mutant (dotted line). Kinetic traces measured by the absorbance at 600 nm (a) and at 330 nm (b). Residuals are from triple-exponential fits (upper plots for CotA and lower plots for the C322A mutant)



shown above, the stabilizing effect of copper is similar for both enzymes as are the spectroscopic and catalytic properties of the enzymes. Binding sites in proteins have a dual-stability character, and are often characterized by the presence of regions with low and with high structural stability, in an overall arrangement that contributes for an optimized binding affinity [51]. In most cases the low-stability regions are loops that become stabilized upon ligand binding and covered a significant portion of the ligand after binding, whereas catalytic residues of enzymes are usually located in regions with higher structural stability. Copper has a pivotal role in CotA-laccase stability as well as in other MCOs [6, 8–12] as shown here by the 100-fold faster unfolding rates of apo forms relative to the holo forms, as measured by fluorescence intensity. Copper incorporation in MCOs is, however, a poorly understood process at the molecular level [10, 11, 48–50, 52–54]. The results presented in this study indicate that the disulfide bridge in CotA-laccase should contribute to the stabilization of the loop near the T1 copper centre, highlighted in Fig. 3, providing the necessary frame for the incorporation of the copper ions at the catalytic sites.

**Acknowledgments** Instituto de Biotecnologia e Química Fina and J.S. Cabral are acknowledged for the use of the Pi-Star 180 instrument for stopped-flow kinetic measurements. The European Synchrotron Radiation Facility in Grenoble, France, and the macromolecular crystallography staff are sincerely acknowledged for provision of synchrotron radiation facilities and support. This work was supported by project grants from Fundação para a Ciência e Tecnologia (FCT), Portugal (POCI/BIO/57083/2004 and PTDC/QUI/73027/2006), and the European Comission (BIORENEW-FP6-2004-NMP-NI-4/026456). A.T.F and C.S.S. hold Ph.D. fellowships (SFRH/BD/31444/2006 and SFRH/BD/40586/2007, respectively) from FCT, Portugal.

## References

- Lindley PF (2001) In: Bertini I, Sigel A, Sigel H (eds) *Handbook on metalloproteins*. Dekker, New York, pp 763–811
- Messerschmidt A (1997) *Multi-copper oxidases*. World Science Press, Singapore
- Fernandes AT, Damas JM, Todorovic S, Huber R, Baratto MC, Pogni R, Soares CM, Martins LO (2010) *FEBS J* 277:3176–3189
- Fernandes AT, Soares CM, Pereira MM, Huber R, Grass G, Martins LO (2007) *FEBS J* 274:2683–2694
- Martins LO, Soares CM, Pereira MM, Teixeira M, Costa T, Jones GH, Henriques AO (2002) *J Biol Chem* 277:18849–18859
- Durao P, Chen Z, Fernandes AT, Hildebrandt P, Murgida DH, Todorovic S, Pereira MM, Melo EP, Martins LO (2008) *J Biol Inorg Chem* 13:183–193
- Fernandes AT, Martins LO, Melo EP (2009) *Biochim Biophys Acta* 1794:75–83
- Agostinelli E, Cervoni L, Giartosio A, Morpurgo L (1995) *Biochem J* 306:697–702
- Savini I, D'Alessio S, Giartosio A, Morpurgo L, Avigliano L (1990) *Eur J Biochem* 190:491–495
- Sedlak E, Wittung-Stafshede P (2007) *Biochemistry* 46:9638–9644
- Sedlak E, Ziegler L, Kosman DJ, Wittung-Stafshede P (2008) *Proc Natl Acad Sci USA* 105:19258–19263
- Koroleva OV, Stepanova EV, Binukov VI, Timofeev VP, Pfeil W (2001) *Biochim Biophys Acta* 1547:397–407
- Durao P, Bento I, Fernandes AT, Melo EP, Lindley PF, Martins LO (2006) *J Biol Inorg Chem* 11:514–526
- Brockwell DJ (2007) *Biochem Soc Trans* 35:1564–1568
- Pace CN, Hebert EJ, Shaw KL, Schell D, Both V, Krajcikova D, Sevcik J, Wilson KS, Dauter Z, Hartley RW, Grimsley GR (1998) *J Mol Biol* 279:271–286
- Radestock SG H (2008) *Eng Life Sci* 5:507–522
- Zhou XX, Wang YB, Pan YJ, Li WF (2008) *Amino Acids* 34:25–33
- Alcaraz LA, Jimenez B, Moratal JM, Donaire A (2005) *Protein Sci* 14:1710–1722
- Pozdnyakova I, Wittung-Stafshede P (2001) *Biochemistry* 40:13728–13733
- Wittung-Stafshede P (2004) *Inorg Chem* 43:7926–7933
- Bento I, Martins LO, Gato Lopes G, Armenia Carrondo M, Lindley PF (2005) *Dalton Trans* 3507–3513
- Aasa R, Vanngard T (1975) *J Magn Reson* 19:308–315
- Leslie A (1992) CCP4 Newslett Protein Crystallogr 26
- Leslie AG (2006) *Acta Crystallogr D* 62:48–57
- Collaborative Computational Project, Number 4 (1994) *Acta Crystallogr D* 50:760–763
- Vagin A, Teplyakov A (1997) *J Appl Crystallogr* 30:1022–1025
- Murshudov GN, Vagin AA, Lebedev A, Wilson KS, Dodson EJ (1999) *Acta Crystallogr D* 55:247–255
- Emsley P, Cowtan K (2004) *Acta Crystallogr D Biol Crystallogr* 60:2126–2132
- Bento I, Silva CS, Chen Z, Martins LO, Lindley PF, Soares CM (2010) *BMC Struct Biol* 10:28
- Brenner AJ, Harris ED (1995) *Anal Biochem* 226:80–84
- Solomon EI, Sundaram UM, Machonkin TE (1996) *Chem Rev* 96:2563–2606
- Moser CC, Dutton PL (1996) In: Bendall DS (ed) *Protein electron transfer*. Bios Scientific Publishers, Oxford, pp 1–21
- Enguita FJ, Martins LO, Henriques AO, Carrondo MA (2003) *J Biol Chem* 278:19416–19425
- Karlin KD, Zhu ZY, Karlin S (1997) *Proc Natl Acad Sci USA* 94:14225–14230
- Durao P, Chen Z, Silva CS, Soares CM, Pereira MM, Todorovic S, Hildebrandt P, Bento I, Lindley PF, Martins LO (2008) *Biochim J* 412:339–346
- Eftink MR, Ghiron CA (1977) *Biochemistry* 16:5546–5551
- Somogyi B, Punyiczki M, Hedstrom J, Norman JA, Prendergast FG, Rosenberg A (1994) *Biochim Biophys Acta* 1209:61–68
- Calhoun DB, Vanderkooi JM, Holtom GR, Englander SW (1986) *Proteins* 1:109–115
- Lakowicz JR (1999) *Principles of fluorescence spectroscopy*. Kluwer/Plenum, New York
- Zhang J, Matthews CR (1998) *Biochemistry* 37:14891–14899
- Leckner J, Bonander N, Wittung-Stafshede P, Malmstrom BG, Karlsson BG (1997) *Biochim Biophys Acta* 1342:19–27
- Pozdnyakova I, Guidry J, Wittung-Stafshede P (2001) *Arch Biochem Biophys* 390:146–148
- Bah A, Garvey LC, Ge J, Di Cera E (2006) *J Biol Chem* 281:40049–40056
- Cawthon TR, Poulsen BE, Davidson DE, Andrews D, Hill BC (2009) *Biochemistry* 48:4448–4454
- Choi DW, Zea CJ, Do YS, Semrau JD, Antholine WE, Hargrove MS, Pohl NL, Boyd ES, Geesey GG, Hartsel SC, Shafe PH, McEllistrem MT, Kisting CJ, Campbell D, Rao V, de la Mora AM, Dispirito AA (2006) *Biochemistry* 45:1442–1453
- Taniguchi T, Ichimura K, Kawashima S, Yamamura T, Tachi'iri Y, Satake K, Kihara H (1990) *Eur Biophys J* 18:1–8

47. Hellman NE, Kono S, Mancini GM, Hoogeboom AJ, De Jong GJ, Gitlin JD (2002) *J Biol Chem* 277:46632–46638
48. Blackburn NJ, Ralle M, Hassett R, Kosman DJ (2000) *Biochemistry* 39:2316–2324
49. Galli I, Musci G, Bonaccorsi di Patti MC (2004) *J Biol Inorg Chem* 9:90–95
50. Kataoka K, Kitagawa R, Inoue M, Naruse D, Sakurai T, Huang HW (2005) *Biochemistry* 44:7004–7012
51. Luque I, Leavitt SA, Freire E (2002) *Annu Rev Biophys Biomol Struct* 31:235–256
52. Davis-Kaplan SR, Askwith CC, Bengtzen AC, Radisky D, Kaplan J (1998) *Proc Natl Acad Sci USA* 95:13641–13645
53. Kwok EY, Severance S, Kosman DJ (2006) *Biochemistry* 45:6317–6327
54. Shi X, Stoj C, Romeo A, Kosman DJ, Zhu Z (2003) *J Biol Chem* 278:50309–50315
55. Laskowski RA, MacArthur MW, Moss DS, Thornton JM (1993) *J Appl Crystallogr* 26:283–291